Bulletin of the Seismological Society of America, Vol. 97, No. 2, pp. 379–388, April 2007, doi: 10.1785/0120060115

Estimating Local V_p/V_s Ratios within Similar Earthquake Clusters

by Guoqing Lin and Peter Shearer

Abstract We develop and test a method to estimate local V_p/V_s ratios for compact similar earthquake clusters using the precise *P* and *S* differential times obtained using waveform cross-correlation. We demonstrate how our technique works using synthetic data and evaluate likely errors arising from near-source takeoff angle differences between *P* and *S* waves. We use a robust misfit function method to compute V_p/V_s ratios for both synthetic data sets and several similar event clusters in southern California, and use a bootstrap resampling approach to estimate standard errors for real data. Our technique has higher resolution for near-source V_p/V_s ratios than typical tomographic inversion methods and provides constraints on near-fault rock properties.

Introduction

Recently, waveform cross-correlation has become an increasingly important tool for improving relative earthquake locations, characterizing event similarity and studying earthquake source properties (e.g., Nakamura, 1978; Poupinet *et al.*, 1984; Got *et al.*, 1994; Dodge *et al.*, 1995; Nadeau *et al.*, 1995; Gillard *et al.*, 1996; Shearer, 1997, 1998; Rubin *et al.*, 1999; Waldhauser *et al.*, 1999; Astiz *et al.*, 2000; Astiz and Shearer, 2000; Shearer, 2002; Shearer *et al.*, 2003; Hauksson and Shearer, 2005; Schaff and Waldhauser, 2005; Shearer *et al.*, 2005). Relative earthquake locations have been remarkably improved by using the very precise differential travel times obtained from waveform cross-correlation, which can often be measured to millisecond precision for similar events, allowing relative earthquake location to be precise to a few meters. In most of these studies, the relative locations are obtained by using a fixed seismic velocity model, although recently the differential times have also been used to constrain tomographic inversions (Zhang and Thurber, 2003).

Here we show that when both *P*- and *S*-wave differential times are available, it is possible to estimate the local *P*-to-*S* velocity ratio within individual similar event clusters in addition to improving the relative locations among the events. Phillips *et al.* (1992) presented a similar technique for microearthquake cluster structure studies but have not yet published the details of their method. We demonstrate that in many cases reasonable V_p/V_s estimates can be obtained even given uncertainties in the *P*- and *S*-takeoff angles. Finally, we use a robust fitting method to handle the outliers that are often present in real data and apply bootstrap resampling to evaluate likely errors. We test our approach on both synthetic data and waveform cross-correlation data for similar event clusters in southern California.

Theory

We begin by considering an idealized example of a single pair of events and then systematically add the complexities associated with more realistic geometries.

Obtaining the V_p/V_s Ratio for a Single Pair of Events

Consider a pair of nearby events, event 1 and event 2, recorded at *n* stations. If the event separation is small enough compared with the source–receiver distances, the differential *P*-wave travel time δT_p^i between these two events at station *i* can be expressed as:

$$\delta T_p^i = T_{p_2}^i - T_{p_1}^i = \frac{\delta l_p^i}{V_p} \tag{1}$$

where $T_{p_2}^i$ and $T_{p_1}^i$ are the source–receiver travel times for events 2 and 1, respectively, δl_p^i is the difference in the ray-path distances between the two events, and V_p is the local *P*-wave velocity (see Fig. 1). Note that because of source–receiver reciprocity this travel-time difference is identical with that resulting from a source at the station generating a wavefront that is recorded at the two event locations. We assume that the events are sufficiently close together that the seismic velocity is locally constant and that the *P*-reciprocal wavefront from each station may be approximated as planar. Because the stations are in different directions, the δl_p^i values will vary among the stations.

Under similar assumptions, the differential *S* travel time may be expressed as

$$\delta T_s^i = T_{s_2}^i - T_{s_1}^i = \frac{\delta l_s^i}{V_s}. \tag{2}$$

Provided that the *P*- and *S*-ray paths are coincident (we will discuss this assumption in greater detail in a later section), then $\delta l_p^i = \delta l_s^i$ and

$$\frac{V_p}{V_s} = \frac{\delta T_s^i}{\delta T_p^i} \tag{3}$$

and we could estimate the local V_p/V_s ratio near the events separately from the δT_s^i and δT_p^i times. Given a number of different stations, the $(\delta T_p^i, \delta T_s^i)$ points ($i = 1, 2, 3, \ldots, n$) should all lie on the $\delta T_s = (V_p/V_s)\delta T_p$ line.

However, we do not normally measure the travel times, T, because we do not know the event origin times. Instead, we measure the arrival times, t. Let δt_0 be the difference in origin times between these two events, that is,

$$\delta t_0 = t_{0_2} - t_{0_1} \tag{4}$$

where t_{0_2} is the origin time of event 2 and t_{0_1} is the origin time of event 1. Then for station i, $t_{p_1}^i = t_{0_1} + T_{p1}^i$, $t_{p_2}^i = t_{0_2} + T_{p2}^i$, and

$$t_{p_2}^i - t_{p_1}^i = (t_{0_2} + T_{p2}^i) - (t_{0_1} + T_{p1}^i) \tag{5}$$

$$= (t_{0_2} - t_{0_1}) + (T_{p_2}^i - T_{p_1}^i) \tag{6}$$

and we have $\delta t_p^i = \delta t_0 + \delta T_p^i$ or $\delta T_p^i = \delta t_p^i - \delta t_0$. Similarly for the S waves we have $\delta T_s^i = \delta t_s^i - \delta t_0$, and thus

$$\frac{V_p}{V_s} = \frac{\delta t_s^i - \delta t_0}{\delta t_p^i - \delta t_0} \tag{7}$$

The effect of the difference in origin times, δt_0, is to shift the $(\delta T_p^i, \delta T_s^i)$ points in both coordinates by δt_0 or along a 45° line. Figure 2 shows the relation between $(\delta t_p^i, \delta t_s^i)$ and $(\delta T_p^i, \delta T_s^i)$.

Equation (7) can be rewritten in the slope–intercept form

$$\delta t_s^i = \left(\frac{V_p}{V_s}\right) \delta t_p^i + \delta t_0 \left(1 - \frac{V_p}{V_s}\right) \tag{8}$$

and we see that the $(\delta t_p^i, \delta t_s^i)$ points are on a line with slope V_p/V_s and y intercept $\delta t_0(1 - V_p/V_s)$ (shown in Fig. 2). Notice that the $\delta t_0(1 - V_p/V_s)$ term does not contain additional constraints on the V_p/V_s ratio because δt_0 is not known *a priori*. Thus, the $(\delta t_p, \delta t_s)$ points for a single pair of events recorded by many stations should form a line with a slope that provides the V_p/V_s ratio and a y intercept that gives the differential origin time. If noise or picking errors are present, then some kind of fitting procedure will be necessary to determine the best-fitting slope and estimate the V_p/V_s ratio. Note that this method can only be used to solve for local V_p/V_s ratios, not the absolute P- or S-wave velocity, unless δl_p^i or δl_s^i is independently known (e.g., Fitch, 1975). In general, these event separation distances and the overall size of an event cluster trade off with the local P or S velocity.

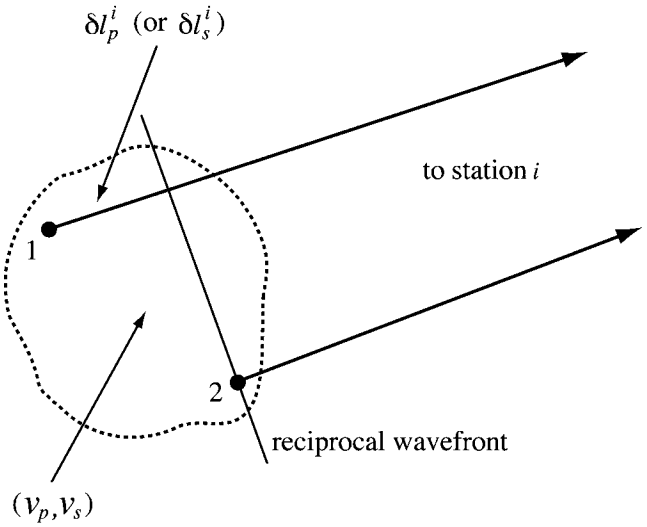

Figure 1. The ray geometry for a pair of events recorded by a distant station.

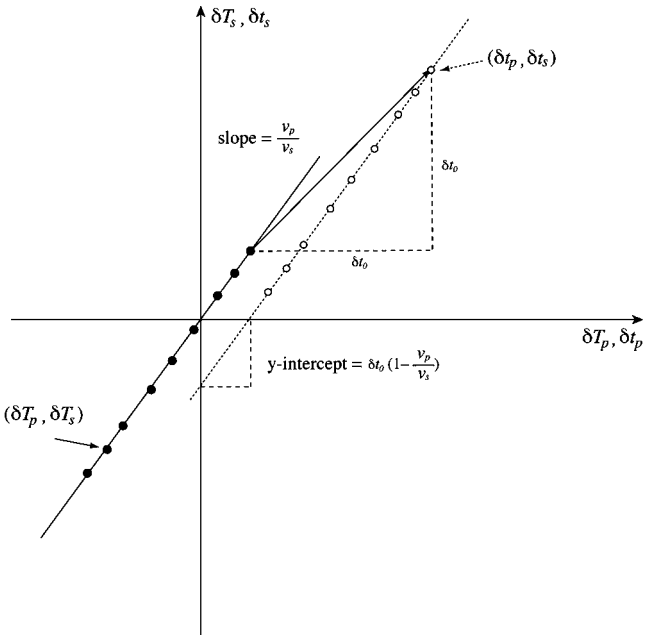

Figure 2. The filled circles show the differential P and S *travel* times and the open circles indicate the differential P and S *arrival* times, which are shifted δt_0 in both coordinates from the P and S travel-time line. The slopes of both lines are the local V_p/V_s ratio. The travel-time line passes through the origin (0, 0), and the arrival-time line has a y intercept of $\delta t_0(1 - V_p/V_s)$.

However, in principle the V_p/V_s ratio can be recovered even without accurate event locations as we demonstrate here.

Next, we use synthetic data to illustrate the technique. We perform our synthetic tests in a 64 × 64 × 32 km uniform half-space with a P-wave velocity of 6 km/sec and

a V_p/V_s ratio of 1.732. We generate a single pair of events separated by 0.2 km with their center at 10 km depth and 20 random station locations on the surface of the half-space. We compute the differential times from this event pair to all 20 stations and use these differential times to estimate the local V_p/V_s ratio. For simplicity, we do not add any noise for this example. Figure 3 shows the synthetic differential times, which, as expected define a line of slope 1.732.

V_p/V_s Ratio for a Cluster of Events

For a single pair of events, equation (8) works directly because the y intercept, $\delta t_0(1 - V_p/V_s)$, is a constant for all the records. But for different pairs of events, it is not appropriate to use equation (8) because the differential origin times are not the same. In other words, for all pairs of events in a compact cluster, assuming they all have the same local V_p/V_s ratios, if we plot all the $(\delta t_p, \delta t_s)$ points on one single plot, they will lie on different straight lines parallel to each other at slope V_p/V_s, but with different y intercepts.

This is illustrated in another synthetic example. In this case, we continue using a uniform half-space model with a P-wave velocity of 6 km/sec and a V_p/V_s ratio of 1.732. We generate 20 random station locations on the surface of the half-space and 27 events with random origin times in a compact $0.2 \times 0.2 \times 0.2$ km cube with the center at 10 km depth. Figure 4 shows the event and station distributions for this test. We compute all possible differential times from each pair of events to the 20 stations (at this stage we still do not include any noise). Figure 5a shows the $(\delta t_p, \delta t_s)$ points for different pairs of events. For plotting purposes, we only plot the points with absolute values less than 0.05 sec. These points are on different lines parallel to each other at the slopes of the true V_p/V_s ratio (1.732) for the cube, but different y intercepts, which are due to the differing differential origin times between event pairs.

To estimate the local V_p/V_s ratio for the compact cube using the differential times from all available event pairs, we can use equation (8) to write a series of equations for each station that records the pair of events 1 and 2:

$$\delta t_s^1 = \left(\frac{V_p}{V_s}\right)\delta t_p^1 + \delta t_0\left(1 - \frac{V_p}{V_s}\right) \quad \text{for station 1} \tag{9}$$

$$\delta t_s^2 = \left(\frac{V_p}{V_s}\right)\delta t_p^2 + \delta t_0\left(1 - \frac{V_p}{V_s}\right) \quad \text{for station 2} \tag{10}$$

$$\vdots$$

$$\delta t_s^n = \left(\frac{V_p}{V_s}\right)\delta t_p^n + \delta t_0\left(1 - \frac{V_p}{V_s}\right) \quad \text{for station } n \tag{11}$$

If we sum these equations and divide by the number of stations n, we then have

$$\delta \bar{t}_s = \left(\frac{V_p}{V_s}\right)\delta \bar{t}_p + \delta t_0\left(1 - \frac{V_p}{V_s}\right) \tag{12}$$

where $\delta \bar{t}_s$ and $\delta \bar{t}_p$ are the mean values of the differential S and P times from all the stations. Subtracting (12) from (8), we obtain

$$(\delta t_s^i - \delta \bar{t}_s) = \left(\frac{V_p}{V_s}\right)(\delta t_p^i - \delta \bar{t}_p) \tag{13}$$

$$\hat{\delta} t_s^i = \left(\frac{V_p}{V_s}\right)\hat{\delta} t_p^i \tag{14}$$

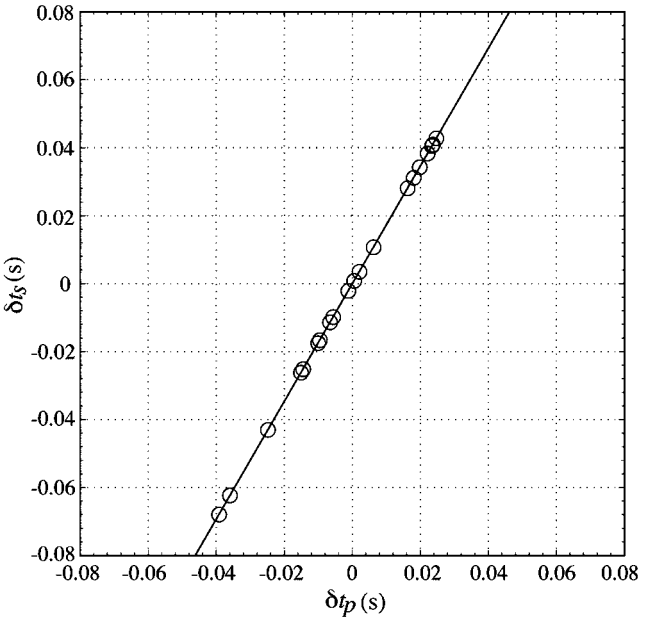

Figure 3. *P* differential arrival times versus *S* differential arrival times for a single pair of events recorded by 20 random stations on the surface. The straight line passing through the points is the best-fitting line from our iterative total least-squares method. The slope of the line is 1.732, which is the true V_p/V_s ratio in our test.

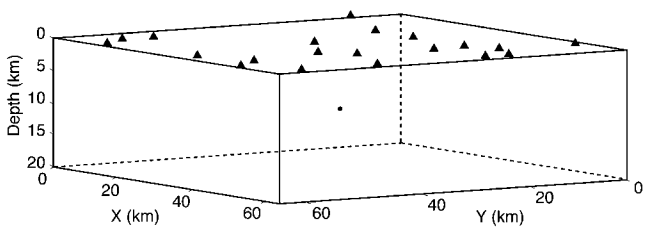

Figure 4. Event and station distributions for the 27 synthetic events in a cube and 20 stations on the surface. The small dot in the middle of the half-space is the cube of events, which is hard to distinguish because the size of the cube is $0.2 \times 0.2 \times 0.2$ km. The triangles are the stations.

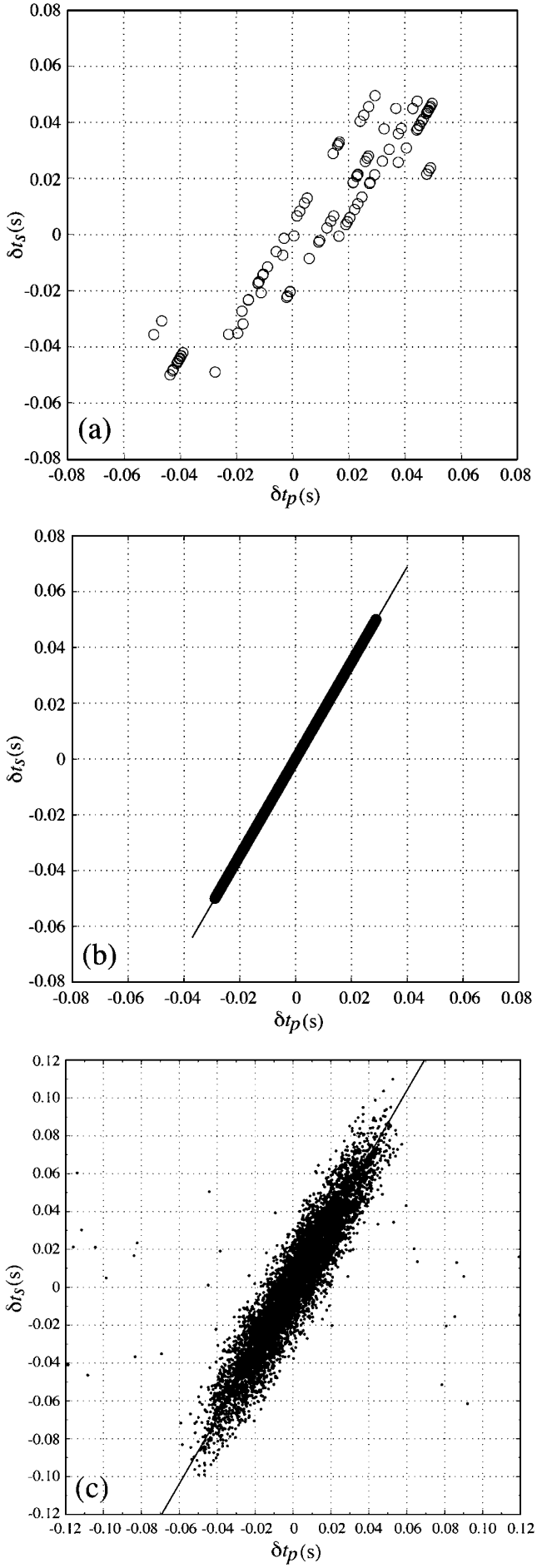

Figure 5. (a) P differential arrival times δt_p versus S differential arrival times δt_s for different pairs of events in a compact cluster. These points are on different lines parallel to each other, with the same slope as the true V_p/V_s ratio for the cluster, but with different y intercepts, which are due to the varying differential origin times. (b) Demeaned δt_p versus demeaned δt_s in (a). These points align on a straight line at slope V_p/V_s and through the origin (0, 0). (c) Demeaned δt_p versus δt_s for 27 synthetic events using the uniform half-space velocity model. We add Gaussian distributed picking errors in both P and S differential times and also uniform distributed errors in P times to simulate the outliers in real data. The slope of the best-fitting straight line is 1.730, which is very close to the true V_p/V_s ratio for the cube.

where $\hat{\delta}t_s^i$ and $\hat{\delta}t_p^i$ are the demeaned differential S- and P-arrival times. In this way we can estimate the V_p/V_s ratio using the $\hat{\delta}\mathbf{t_p}$ and $\hat{\delta}\mathbf{t_s}$ vectors from all event pairs in the compact cluster. Because equation (14) is not a function of differential origin times, if we assume all pairs of events are in a compact cluster, all the $(\hat{\delta}t_p,\ \hat{\delta}t_s)$ points in the cluster should align on a straight line at slope V_p/V_s and through the origin (0, 0), as shown in Figure 5b. This makes it possible to fit all of the points simultaneously for the best-fitting V_p/V_s ratio for the entire cluster.

Fitting Method for Noisy Data

In the preceding synthetic examples we have not included any noise, so the data points directly define the line that gives the V_p/V_s ratio. However, real data will have some degree of error, which will require the use of a fitting method to compute the best-fitting line. In addition, our differential time data often have obvious outliers—extreme values that would severely bias any conventional least-squares approach. We thus apply a more robust method, which measures distance using the L_2 norm for data misfits below some specified value, $d_{\max}$ (which in general will depend on the observations), and an L_1 norm for larger values. This hybrid $l^1 - l^2$ error measure was proposed by Huber (1973) and can be used to compute what we will term the *robust mean* of a distribution. For data with outliers, we use the robust mean to demean the differential S- and P-arrival times for each station as described previously.

In the classical least-squares (LS) line-fitting approach, one of the two measurements is assumed to be exact and free of error and a regression is performed to find the best-fitting line to the second measurement. For example, if the the data are given as (x, y) pairs and the error is assumed to be entirely in y, then we find the slope and y intercept that minimize the sum of the squares of the vertical (y) distances between the line and the data. In our case, however, we likely have errors in both the δt_s^i and δt_p^i values. If the x and y errors are assumed equal, then the optimal solution is given by the line with the minimum perpendicular distance to each point.

Least-squares solutions to this problem are described in, for example, Jefferys (1981), Press *et al.* (1992), and Van Huffel (1997). In the case of unequal x and y errors, the problem can be rescaled to be equivalent to the equal error case. To account for outliers in our differential time measurements, we modify this method to be more robust. We perform a grid search for lines of different slopes, computing the best-fitting y intercept for each line from the robust mean of the perpendicular distances to each data point, after first scaling the δt_s^i values so that their expected variance matches that of the δt_p^i values.

As we will discuss subsequently, biases resulting from angular differences in the local P- and S-ray paths near the events will cause errors in the δt_s points to be R times greater than the errors in the δt_p points, where R is the V_p/V_s ratio. We thus multiply the data δt_s values by $1/R$ so that their expected error is similar in size to the δt_p error. Note, however, that any desired rescaling could be applied at this point if the relative variance of δt_p and δt_s measurements is known *a priori*. Because our method is solving for R, an iterative method is necessary. We assume a starting value for R, find the best-fitting line, and then replace R with its updated value ($R = R \times$ slope) for the next iteration. This iterative algorithm converges after several (3 to 5) iterations, and the final R value is our estimate for the V_p/V_s ratio. For our synthetic tests with noise, we use 1.0 as an initial value for R to test the robustness of our method; but for real data, 1.732 would be a more reasonable starting value for the V_p/V_s ratio, and is used in our analysis of waveform cross-correlation results.

To test our fitting method, we generate a synthetic data set for the 27 events in a cube and 20 stations on the surface using the same uniform half-space velocity model in the previous example. We add Gaussian distributed noise with zero mean and a standard deviation of 5 msec, which is comparable to the size of the scatter in real cross-correlation data, for the P differential times and scaled by 1.732 (the true V_p/V_s ratio) for the S differential times. To simulate the outliers in real data, we also add uniform distributed noise in 1% of the P differential times. To show that our iterative method works correctly even if the initial R estimate is incorrect, we assume $R = 1$ in the first iteration. We test different initial values for R (between 0.1 and 10) in our study and find they all converge to the same V_p/V_s ratio for this synthetic example. Figure 5c shows the resulting data points and our V_p/V_s ratio estimate of 1.730. If we used the classical least-squares approach rather than our robust method, the estimated V_p/V_s ratio is 1.583. If the errors in the δt_p and δt_s points are assumed to be equal, then the robust total least-squares result is biased and we obtain a V_p/V_s ratio of 1.784 for this example.

Effect of Different Takeoff Angles for P and S

So far we have been assuming that the P and S waves are coincident so that they have the same takeoff angles. Now we consider the possible errors that may result if the P- and S-takeoff angles are different. This might be caused by depth-varying V_p/V_s differences or by local V_p/V_s variations near the source pair.

First, let us consider the effect that ray-path deviations will have on our δt_p and δt_s measurements. The ray-angle geometry at the event pair is shown in Figure 6. Let $\hat{\mathbf{a}}_p$ be the P-ray unit direction vector, $\hat{\mathbf{a}}_s$ be the S-ray unit direction vector, 2ε be the angle between $\hat{\mathbf{a}}_p$ and $\hat{\mathbf{a}}_s$, and $\hat{\mathbf{e}}$ be the unit direction vector from event 1 to event 2. Without loss of generality we may assume that $\hat{\mathbf{a}}_p$ and $\hat{\mathbf{a}}_s$ are in the x-z plane and symmetric about the z axis. We can then write

$$\hat{\mathbf{a}}_p = (-\sin\varepsilon,\ 0,\ \cos\varepsilon) \tag{15a}$$

$$\hat{\mathbf{a}}_s = (\sin\varepsilon,\ 0,\ \cos\varepsilon) \tag{15b}$$

$$\hat{\mathbf{e}} = (\sin\theta\cos\phi,\ \sin\theta\sin\phi,\ \cos\theta) \tag{15c}$$

where the event vector $\hat{\mathbf{e}}$ has an arbitrary orientation defined by the polar angle θ and the azimuthal angle ϕ. Let β_p be the angle between $\hat{\mathbf{a}}_p$ and $\hat{\mathbf{e}}$, and β_s be the angle between $\hat{\mathbf{a}}_s$ and $\hat{\mathbf{e}}$. We then have

$$\cos\beta_p = \hat{\mathbf{a}}_p \cdot \hat{\mathbf{e}} = -\sin\varepsilon\sin\theta\cos\phi + \cos\varepsilon\cos\theta \tag{16a}$$

$$\cos\beta_s = \hat{\mathbf{a}}_s \cdot \hat{\mathbf{e}} = \sin\varepsilon\sin\theta\cos\phi + \cos\varepsilon\cos\theta \tag{16b}$$

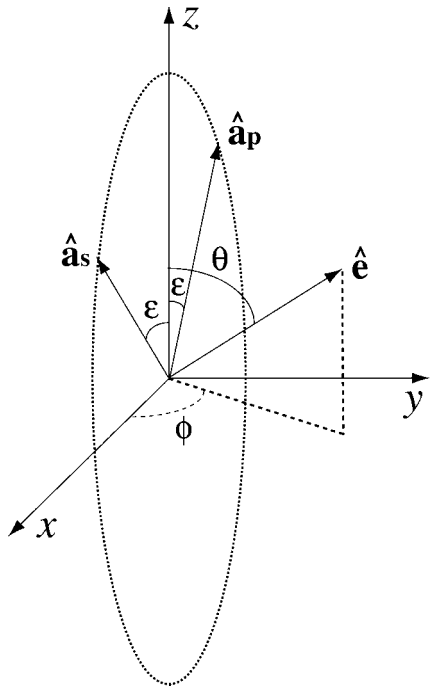

Figure 6. The spherical coordinate system that we use to show the bias in δt_p and δt_s due to ray-path deviations.

We can express the differential P and S travel times as

$$\delta t_p = (\hat{\mathbf{a}}_p \cdot \mathbf{e})/V_p = (\|\mathbf{e}\|\, \hat{\mathbf{a}}_p \cdot \hat{\mathbf{e}})/V_p = (\|\mathbf{e}\| \cos \beta_p)/V_p \quad (17a)$$

$$\delta t_s = (\hat{\mathbf{a}}_s \cdot \mathbf{e})/V_s = (\|\mathbf{e}\|\, \hat{\mathbf{a}}_s \cdot \hat{\mathbf{e}})/V_s = (\|\mathbf{e}\| \cos \beta_s)/V_s \quad (17b)$$

where $\|\mathbf{e}\|$ is the distance between event 1 and event 2 (i.e., $\mathbf{e} = \|\mathbf{e}\|\hat{\mathbf{e}}$. Thus, each $(\delta t_p, \delta t_s)$ point can be written as

$$(\delta t_p, \delta t_s) = \|\mathbf{e}\|\left(\frac{\cos \beta_p}{V_p}, \frac{\cos \beta_s}{V_s}\right) = \|\mathbf{e}\|\left(\frac{\cos \varepsilon \cos \theta}{V_p} - \frac{\sin \varepsilon \sin \theta \cos \phi}{V_p}, \frac{\cos \varepsilon \cos \theta}{V_s} + \frac{\sin \varepsilon \sin \theta \cos \phi}{V_s}\right) \quad (18)$$

When the P- and S-ray paths are coincident (i.e., $\varepsilon = 0$), then the slope of the $(\delta t_p, \delta t_s)$ points is equal to V_p/V_s ratio. When ε is small but nonzero, then $\cos \varepsilon \approx 1$, so that δt_p and δt_s are biased from their $\varepsilon = 0$ values by $(\sin \varepsilon \sin \theta \cos \phi)/V_p$ and $(\sin \varepsilon \sin \theta \cos \phi)/V_s$, respectively. Thus, we see that the bias introduced into the δt_s differential times by ray-path deviations will be a factor V_p/V_s times larger than the bias in the δt_p times.

To show the effect of different P- and S-wave takeoff angles, we generate a velocity model in which both V_p and V_s increase, but the V_p/V_s ratio decreases with depth (see Fig. 7). At 10 km source depth and 30 km epicentral distance, the P-takeoff angle at the source is 80.13° (from vertical) and the S-takeoff angle is 85.03°. We use the depth-varying velocity model to generate differential times for a single pair of events separated by 0.2 km at 10 km depth with the event separation vector perpendicular to the surface, and recorded by 20 random stations at the surface. The epicentral distances range between 5 km and 38 km, most of which are about 30 km. In Figure 8, we plot $(\delta t_p, \delta t_s)$ points for this pair of events. For the purpose of this test, we do not add any random noise to the differential times. The true local V_p/V_s ratio at the center of the events is 1.697, whereas the estimated slope is 1.830. The points are biased from the true straight line because the takeoff angles for P and S from each station are different.

The bias in the estimated V_p/V_s ratio will vary depending on the orientation of the event pair with respect to the incoming rays. To illustrate this, we use the same depth-varying velocity model and station distribution, but rotate the relative location vector of the pair of events every 5° uniformly in three dimensions while keeping the center of the events fixed. In this way, the P- and S-takeoff angles from each station to the pair of events change in all possible directions. We then use the $(\delta t_p, \delta t_s)$ points from all these rotated pairs of events to estimate the slope.

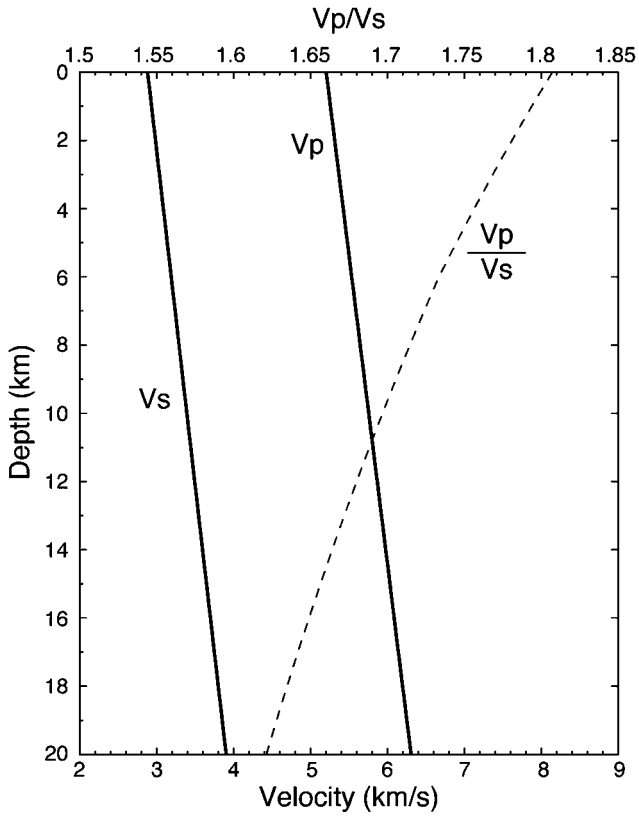

Figure 7. The velocity model that we use to test the effect of different P- and S-wave takeoff angles.

Figure 9 shows all these points from the rotated event pairs and the best-fitting straight line. The slope of the best-fitting line is 1.697, which is the true V_p/V_s ratio at the center of the events. Thus, although P- versus S-takeoff angle differences will bias results for individual event pairs, this bias will tend to average out when a large number of random event orientations are present. This can be seen from symmetry considerations in Figure 6 and equation (18); for every $\hat{\mathbf{e}}_1$ vector with a positive V_p/V_s bias, there will also exist a corresponding $\hat{\mathbf{e}}_2$ vector with negative bias at $\phi_2 = \phi_1 + \pi$.

For real data it is not possible to do the three-dimensional rotations. However, if an event cluster is small and contains event pairs of varying orientations and the station distribution is good enough, the ray paths for all the events in the cluster may form a random distribution of directions, as in the three-dimensional rotations, so that the local V_p/V_s ratio may be accurately recorded. To show this, we generate the synthetic differential times for the 27 events in the cube and 20 stations in the previous section using the same depth-varying velocity model. The V_p/V_s ratio at the center of the cube is 1.697. The event and station distributions are shown in Figure 4. The $(\delta t_p, \delta t_s)$ points for this small cube are shown in Figure 10. The slope of the best-fitting straight line is 1.697, which is the true V_p/V_s ratio at the center of the cube.

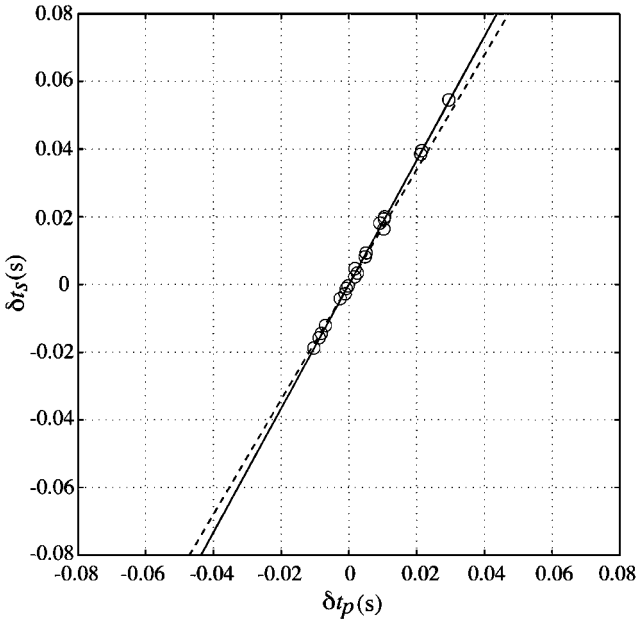

Figure 8. δt_p versus δt_s for a single pair of events recorded by 20 stations at the surface using the depth-varying velocity model of Figure 7. The estimated slope is 1.830, shown by the solid line, while the true local V_p/V_s ratio is 1.697, shown by the dashed line.

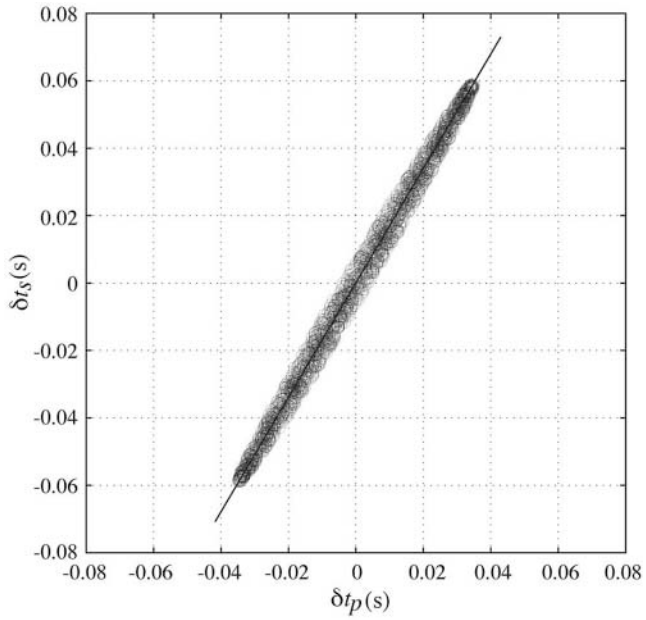

Figure 9. δt_p versus δt_s for the same station distribution and velocity model used in Figure 8. In this case, we rotate the pair of events every 5° uniformly in three dimensions so that the ray paths from the stations change in all possible directions. For plotting purposes, we only plot a random 5% of the points. The estimated slope is 1.697, which is the true V_p/V_s ratio at the cluster depth.

However, it should be recognized that the bias may not be completely removed in the case of event clusters with a more limited distribution of events. For example, if the 27 events in this synthetic example are restricted to a horizontal plane, then the V_p/V_s ratio estimate is 1.716. If the events are located within a vertical plane, then the computed V_p/V_s ratio will vary between 1.677 and 1.689, depending on the azimuth of the plane. This suggests that the most accurate results for real data clusters will be obtained for clusters with a three-dimensional distribution of events.

As a final test of our V_p/V_s ratio estimate approach, we generate a synthetic data set for the 27 events in a cube and 20 stations on the surface using the same depth-varying velocity model in the previous example. We add Gaussian distributed noise with zero mean and standard deviations of 5 msec for the *P* differential times and scaled by 1.697 (the true V_p/V_s ratio) for the *S* differential times. To simulate the outliers in real data, we also add uniform distributed noise in 5% of the *P* differential times. Our V_p/V_s ratio estimate for this cube is 1.692 (shown in Fig. 11), very close to the true value of 1.697. Note that the outliers in our test are very strong, which would significantly bias the ratio estimate if we used simple least squares rather than our robust approach. The V_p/V_s ratio estimate from simple least squares is 1.243 for this example. If the errors in the δt_p and δt_s points are assumed to be equal, then the robust total least-squares result is biased and we obtain a V_p/V_s ratio of 1.752.

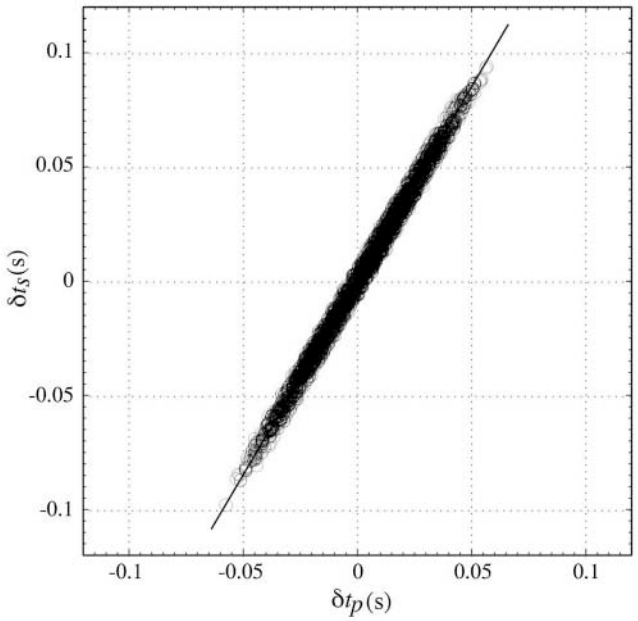

Figure 10. δt_p versus δt_s for 27 synthetic events using the velocity model shown in Figure 7. The slope of the best-fitting straight line is 1.697, which is the true V_p/V_s ratio for the cube.

Examples for Southern California Earthquake Clusters

We apply this V_p/V_s ratio estimate method to differential times from waveform cross-correlation for two similar event clusters in southern California taken from Shearer *et al.* (2005). To estimate the V_p/V_s ratio for each event cluster accurately, we use event pairs with at least five differential *P-S* times and require more than 100 differential *P-S* time pairs for the entire cluster.

Estimating Standard Errors

For real data, the event and station distributions may not be as good as in our synthetic data, so it is desirable to estimate standard errors in our V_p/V_s ratios. Since the true values are unknown, certain assumptions are necessary to obtain error estimates. The classical least-squares method can be used to compute error ellipses based upon χ^2 misfit criteria and is optimal for the case of uncorrelated Gaussian random errors. These methods are not easily generalized to other model norms, such as the robust least-squares method that is used here. As an alternative, we have applied a bootstrap approach (Efron and Gong, 1983; Efron and Tibshirani, 1991), in which each pair of suitable differential *P* and *S* times in the same cluster may be sampled multiple times or not sampled at all. This process is repeated for 100 subsamples for each cluster and we estimate the standard deviation of these 100 subsamples as the standard error of the V_p/V_s ratio. However, note that these formal statistical uncertainties (which can be quite small when the number of data points is large) represent a minimum error because they do not include the possible biases resulting from *P*- and *S*-takeoff angle differences in nonisotropic event distributions.

V_p/V_s Ratio Estimates Using Waveform Cross-Correlation Results

Here we present two examples of V_p/V_s ratio estimates using the waveform cross-correlation results for clusters in southern California taken from Shearer *et al.* (2005). Figure 12 shows the 7265 demeaned (δt_p, δt_s) points for cluster 99 (in the POLY5 subset of events) in southern California from Shearer *et al.* (2005). The centroid of this cluster is at (33.511° N, −116.555° E, 10.1 km). The slope of the best-fitting straight line is 1.782 and the standard deviation of our V_p/V_s ratio estimate from bootstrap resampling is 0.006. Figure 13 shows the 5520 demeaned (δt_p, δt_s) points for cluster 427 in POLY5. The centroid of this cluster is at (33.478° N, −116.495° E, 10.5 km). The resolved V_p/V_s ratio for this cluster is 1.713 and the standard deviation from bootstrap resampling is 0.010. In principle, these observed V_p/V_s ratios could be used to constrain the lithology of the rock in the source regions. As noted by Tatham (1982), laboratory and well-log data suggest a V_p/V_s ratio near 1.8 for dolomite and in the range of 1.6 to 1.75 for sandstones. However, the

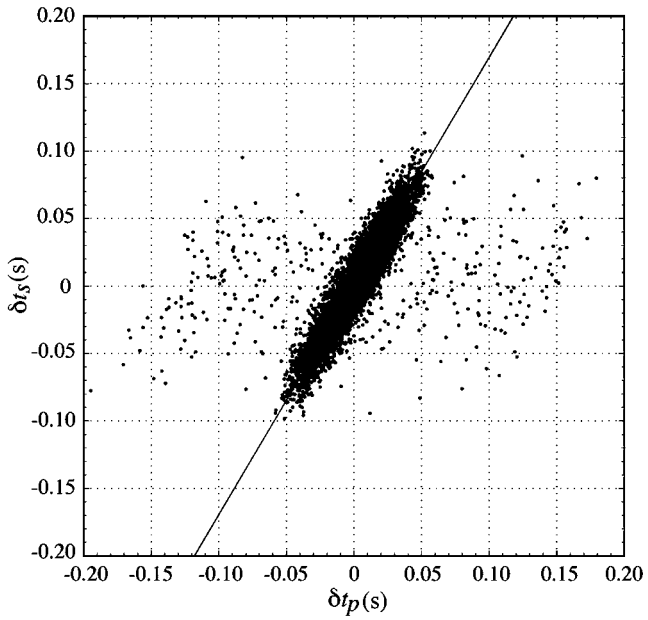

Figure 11. δt_p versus δt_s for 27 synthetic events using the velocity model shown in Figure 7. We add Gaussian distributed picking errors in both *P* and *S* differential times and also uniform distributed errors in *P* times to simulate the outliers in real data. The slope of the best-fitting straight line is 1.692, which is very close to the true V_p/V_s ratio for the cube.

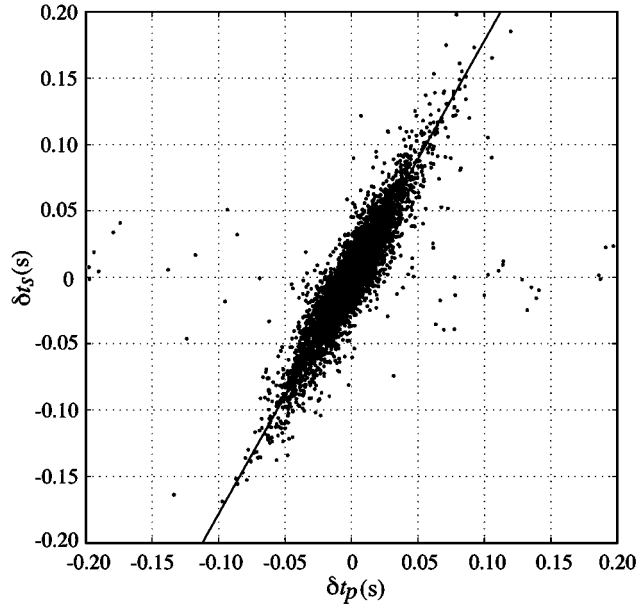

Figure 12. Demeaned δt_p versus δt_s for the 74 events in cluster 99 from the SHLK catalog (Shearer *et al.*, 2005). The slope of the best-fitting straight line is 1.782 ± 0.006.

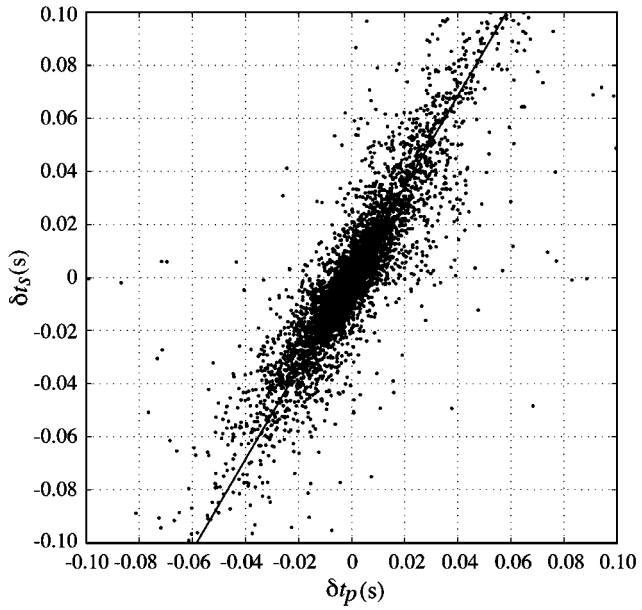

Figure 13. Demeaned δt_p versus δt_s for the 81 events in cluster 427 from the SHLK catalog (Shearer *et al.*, 2005). The slope of the best-fitting straight line is 1.713 ± 0.010.

presence of cracks and the degree of pore fluid saturation can also be important factors in determining the V_p/V_s ratio.

Discussion

In general, variations in V_p/V_s ratios may be determined by using tomographic methods. However, the resolution of local V_p/V_s ratios from tomography is usually limited due to the coarse grid sizes, although Zhang and Thurber (2005) showed that the adaptive mesh tomography scheme has the ability to resolve the velocity structure near the source region. In this study, we develop a method to estimate local V_p/V_s ratios for event clusters by using precise differential times derived from the waveform cross-correlation technique. Our method is simple to execute and does not require much computer power. The uncertainty is typically small since the precision of differential times from waveform cross-correlation can be as small as a millisecond and the V_p/V_s ratio can be recovered even without accurate event locations.

For real data, the $l^1 - l^2$ misfit measure is useful to reduce the effects of outliers. Due to possible differences in *P*- and *S*-wave takeoff angles, the estimated V_p/V_s ratios could be biased from their true values. However, as shown in our synthetic data tests, if the seismic ray coverage for a cluster of events is good enough, the true V_p/V_s ratio can still be recovered. We find that the resolved V_p/V_s ratios are very sensitive to the differential times, especially at short hypocentral distances where the *P* and *S* arrivals are very close to each other. In this case, the *S* waveforms should be windowed very carefully, because otherwise the V_p/V_s ratios will likely be underestimated because part of the *P* wave train may be included in the *S*-wave cross-correlation.

In this study, we assume that the scale length of changes in V_p/V_s ratios is greater than the size of the similar event clusters. Our method could be biased if there are significant variations in the V_p/V_s ratio within the cluster, although given a good distribution of events we should still obtain a reasonable value for the average V_p/V_s ratio. It is possible that spatial and/or temporal variations in V_p/V_s ratios could be identified by analyzing subsets of similar event clusters, but we do not attempt this here. Given recent applications of waveform cross-correlation to large earthquake catalogs (e.g., Hauksson and Shearer, 2005; Schaff and Waldhauser, 2005), widespread computation of near-source V_p/V_s ratios appears practical and should provide a useful complement to tomographic methods. In addition, these local V_p/V_s measurements should permit computing more accurate relative locations of events within each similar event cluster. We will defer discussing details of how this can be done to a later study.

Acknowledgments

We thank Egill Hauksson for his involvement in the waveform cross-correlation calculations and Jose Pujol, Nick Rawlinson, and Cliff Thurber for their detailed and constructive reviews. Funding for this research was provided by NEHRP/USGS grant 03HQPA0001. This research was also supported by the Southern California Earthquake Center, which is funded by NSF Cooperative Agreement EAR-0106924 and USGS Cooperative Agreement 02HQAG0008. The SCEC contribution number for this paper is 995.

References

Astiz, L., and P. M. Shearer (2000). Earthquake locations in the inner continental borderland, offshore southern California, *Bull. Seism. Soc. Am.* **90,** 425–449.

Astiz, L., P. M. Shearer, and D. C. Agnew (2000). Precise relocations and stress change calculations for the Upland earthquake sequence in southern California, *J. Geophys. Res.* **105,** 2937–2953.

Dodge, D. A., G. C. Beroza, and W. L. Ellsworth (1995). Foreshock sequence of the 1992 Landers, California, earthquake and its implications for earthquake nucleation, *J. Geophys. Res.* **100,** 9865–9880.

Efron, B., and G. Gong (1983). A leisurely look at the bootstrap, the jackknife and cross-validation, *Am. Statist.* **37,** 36–48.

Efron, B., and R. Tibshirani (1991). Statistical data analysis in the computer age, *Science* **253,** 390–395.

Fitch, T. J. (1975). Compressional velocity in source regions of deep earthquakes: an application of the master earthquake technique, *Earth Planet. Sci. Lett.* **26,** 156–166.

Gillard, D., A. M. Rubin, and P. Okubo (1996). Highly concentrated seismicity caused by deformation of Kilauea's deep magma system, *Nature* **384,** 343–346.

Got, J.-L., J. Fréchet, and F. W. Klein (1994). Deep fault plane geometry inferred from multiplet relative relocation beneath the south flank of Kilauea, *J. Geophys. Res.* **99,** 15,375–15,386.

Hauksson, E., and P. Shearer (2005). Southern California hypocenter relocation with waveform cross-correlation, Part 1: results using the double-difference method, *Bull. Seism. Soc. Am.* **95,** 896–903.

Huber, P. J. (1973). Robust regression: asymptotics, conjectures and monte carlo, *Ann. Statist.* **1,** 799–821.

Jefferys, W. H. (1981). On the method of least squares, II, *Astr. J.* **86,** 149–155.

Nadeau, R. M., W. Foxall, and T. V. McEvilly (1995). Clustering and periodic recurrence of microearthquakes on the San Andreas Fault at Parkfield, California, *Science* **267,** 503–507.

Nakamura, Y. (1978). A_1 moonquakes: source distribution and mechanism, *Proc. Lunar Planet. Sci. Conf.* **9,** 3589–3607.

Phillips, W. S., L. S. House, and M. C. Fehler (1992). Vp/Vs and the structure of microearthquake clusters, *Seism. Res. Lett.* **63,** 56–57.

Poupinet, G., W. L. Ellsworth, and J. Frechet (1984). Monitoring velocity variations in the crust using earthquake doublets: an application to the Calaveras Fault, California, *J. Geophys. Res.* **89,** 5719–5732.

Press, W. H., S. A. Teukolsky, W. T. Vetterling, and B. Flannery (1992). *Numerical Recipes in Fortran 77: The Art of Scientic Computing*, Second Ed., Cambridge University Press, Cambridge.

Rubin, A. M., D. Gillard, and J.-L. Got (1999). Streaks of microearthquakes along creeping faults, *Nature* **400,** 635–641.

Schaff, D. P., and F. Waldhauser (2005). Waveform cross-correlation-based differential travel-time measurements at the Northern California Seismic Network, *Bull. Seism. Soc. Am.* **95,** 2446–2461.

Shearer, P. M. (1997). Improving local earthquake locations using the L1 norm and waveform cross correlation: application to the Whittier Narrows, California, aftershock sequence, *J. Geophys. Res.* **102,** 8269–8283.

Shearer, P. M. (1998). Evidence from a cluster of small earthquakes for a fault at 18 km depth beneath Oak Ridge, southern California, *Bull. Seism. Soc. Am.* **88,** 1327–1336.

Shearer, P. M. (2002). Parallel fault strands at 9-km depth resolved on the Imperial Fault, southern California, *Geophys. Res. Lett.* **29,** doi 10.1029/2002GL015302.

Shearer, P. M., J. L. Hardebeck, L. Astiz, and K. B. Richards-Dinger (2003). Analysis of similar event clusters in aftershocks of the 1994 Northridge, California, earthquake, *J. Geophys. Res.* **108,** B1, 2035, doi 10.1029/2001JB000685.

Shearer, P. M., E. Hauksson, and G. Lin (2005). Southern California hypocenter relocation with waveform cross-correlation, Part 2: results using source-specific station terms and cluster analysis, *Bull. Seism. Soc. Am.* **95,** 904–915.

Tatham, R. H. (1982). V_p/V_s and lithology, *Geophysics* **47,** 336–344.

Van Huffel, S. (1997). *Recent Advances in Total Least Squares Techniques and Errors-in-Variables Modeling*, Society for Industrial and Applied Mathematics, Philadelphia, Pennsylvania.

Waldhauser, F., W. L. Ellsworth, and A. Cole (1999). Slip-parallel seismic lineations on the northern Hayward Fault, California, *Geophys. Res. Lett.* **26,** 3525–3528.

Zhang, H., and C. Thurber (2005). Adaptive mesh seismic tomography based on tetrahedral and Voronoi diagrams: application to Parkfield, California, *J. Geophys. Res.* **110,** B04303, doi 10.1029/2004JB003186.

Zhang, H., and C. H. Thurber (2003). Double-difference tomography: the method and its application to the Hayward Fault, California, *Bull. Seism. Soc. Am.* **93,** 1875–1889.

Institute of Geophysics and Planetary Physics
Scripps Institution of Oceanography
University of California San Diego
La Jolla, California 92093-0225

Manuscript received 22 May 2006.